Sensors and Actuators B xxx (2012) xxx–xxx

Contents lists available at ScienceDirect

Sensors and Actuators B: Chemical

journal homepage: www.elsevier.com/locate/snb

Miniaturized chemical imaging sensor system using an OLED display panel

Ko-ichiro Miyamoto[a,*], Kazumi Kaneko[b], Akira Matsuo[a], Torsten Wagner[b], Shin'ichiro Kanoh[c], Michael J. Schöning[d,e], Tatsuo Yoshinobu[a,b]

[a] Department of Electronic Engineering, Tohoku University, 6-6-05 Aza-Aoba, Aramaki, Aoba-ku, Sendai 980-8579, Japan
[b] Department of Biomedical Engineering, Tohoku University, 6-6-05 Aza-Aoba, Aramaki, Aoba-ku, Sendai 980-8579, Japan
[c] Tohoku Institute of Technology, Taihaku-ku, Sendai 982-8577, Japan
[d] Institute of Nano- and Biotechnologies, Aachen University of Applied Sciences, Heinrich-Mußmann-Str. 1, 52428 Jülich, Germany
[e] Peter-Grünberg Institute (PGI-8), Research Centre Jülich, 52425 Jülich, Germany

ARTICLE INFO

Article history:
Available online xxx

Keywords:
Organic light-emitting diode display
Chemical imaging sensor
Light-addressable potentiometric sensor
LAPS

ABSTRACT

The chemical imaging sensor is a semiconductor-based chemical sensor that can visualize the two-dimensional distribution of specific ions or molecules in the solution. In this study, we developed a miniaturized chemical imaging sensor system with an OLED display panel as a light source that scans the sensor plate. In the proposed configuration, the display panel is placed directly below the sensor plate and illuminates the back surface. The measured area defined by illumination can be arbitrarily customized to fit the size and the shape of the sample to be measured. The waveform of the generated photocurrent, the current–voltage characteristics and the pH sensitivity were investigated and pH imaging with this miniaturized system was demonstrated.

1. Introduction

The chemical imaging sensor [1–4] is a semiconductor sensor which is capable of visualizing the distribution of chemical species in electrochemical and biological samples. It is based on the principle of the light-addressable potentiometric sensor (LAPS) [5], in which the variation of the width of the depletion layer in Si responding to the ion concentration on the sensing surface is read out in the form of a photocurrent induced by illumination of the sensor plate.

The most important advantage of the LAPS measurement is that the measured area can be defined by the light spot, thus a spatially resolved measurement of the ion concentration is possible by using a local illumination. The two-dimensional distribution of chemical species can be obtained as a chemical image by using a scanning laser beam, where the spatial resolution can be enhanced by focusing. We have developed a chemical imaging sensor system based on LAPS, and reported several applications such as monitoring of metabolic activities of *Escherichia coli* colonies [2], or visualization of diffusing ions in an electrochemical system [6].

As described above, the chemical imaging sensor is a powerful tool to visualize the chemical species. Many other applications in the fields of clinical tests or environmental monitoring are proposed. For instance, Stein et al. reported that the metabolic activity of cells cultured on LAPS could be monitored by local illumination [7]. Liu et al. reported on detection of toxic heavy metal ions by monitoring the response of cultured cells by a LAPS-based system [8]. Miniaturization of the chemical imaging sensor system would be a great help in these applications. In conventional systems, however, the need for a focusing optics and a mechanical scan stage hindered the miniaturization of the system.

In this study, we developed a new design of chemical imaging sensor system using an organic LED (OLED) display panel as a light source placed in the proximity of the back surface of the sensor plate. In comparison to the conventional liquid crystal display (LCD), the self-luminous capability of the OLED display is suitable for this purpose due to its higher contrast. In the case of LCD, the leakage of the backlight through gaps between pixels induces undesired photocurrent which is not negligible in LAPS measurement.

Fig. 1 shows the measurement system of the novel OLED-LAPS. The pixels turned on act as a light spot that defines the investigated area. Since the light spot on the display panel can be moved freely, it can replace the laser beam and the mechanical stage of the conventional system. While it takes hundreds of milliseconds to move a laser beam mechanically from one end to another end of the measured area, the light spot on the OLED display can be moved within several milliseconds just by sending a command. As a similar approach, Filippini et al. proposed the use of a computer screen as a light source for surface plasmon resonance imaging [9] and visible absorption spectroscopy [10].

* Corresponding author.
E-mail address: k-miya@ecei.tohoku.ac.jp (K. Miyamoto).

0925-4005/$ – see front matter © 2012 Published by Elsevier B.V.
doi:10.1016/j.snb.2011.02.029

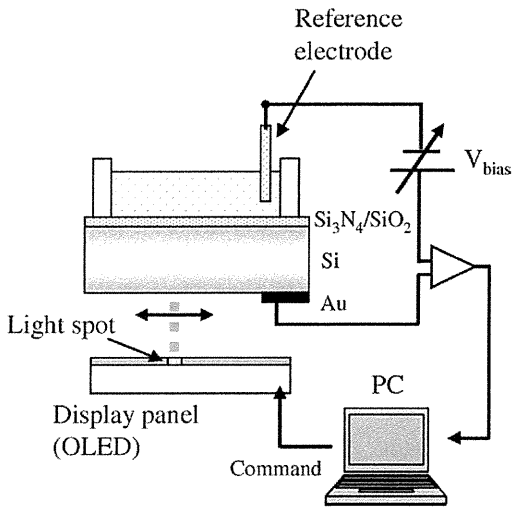

Fig. 1. Schematic diagram of OLED-LAPS system.

Based on the OLED-LAPS, the chemical imaging sensor system can be miniaturized and the cost of the measurement system can be drastically reduced. Besides, not only the position but also the size and the shape of the light spot on the display panel can be changed without mechanical parts and focusing optics. Thus, the measured area defined by illumination can be arbitrarily customized to fit the size and the shape of the sample to be investigated.

2. Experimental setup

Fig. 1 is a schematic view of the measurement system that has been developed in this study. The measurement system consists of a sensor plate, a sample well mounted on the sensor surface, a display panel module to illuminate the sensor plate, and a measurement software. The sensor plate and the sample well were essentially the same as those we used in previous studies [11]. The sensor plate (36 mm × 36 mm) was made of n-type silicon (10–20 Ω cm) with double layer of a 50-nm-thick thermal oxide and a 100-nm-thick silicon nitride deposited by low-pressure chemical vapor deposition (LP-CVD). The surface of the silicon nitride layer functions as a pH-sensitive layer.

A 0.96-inch organic LED display (μOLED-96-G1, 4D Systems Inc.) with a resolution of 96 × 64 (width × height) pixels was used to illuminate the sensor plate. The dimension of a single pixel on the OLED display was 200 μm × 200 μm.

On this OLED display, pixels on the same line flash at the same time, and lines flash one after another with a delay of 116 ns. It takes therefore 116 ns × 64 lines (=7.4 ms) to display an image, which corresponds to a refresh rate of 135 Hz.

The measurement software controls the position and pattern of pixels on the display via USB interface. The measurement software also adjusts the bias voltage applied to the sensor, records the photocurrent while scanning the light spot, and displays the photocurrent distribution as a chemical image. The frequency component corresponding to the refresh rate of the display panel was extracted by Fourier analysis. For the characterization of the pH response of the sensor, the sample was filled with a pH standard solution (Titrisol®, Merck KGaA, Germany).

In the resolution measurement, a test pattern was scanned with different sizes of light spots from 8 × 8 to 1 × 1 pixels. The test pattern (alphabetical letter 'LAPS') was directly drawn on the sensing surface with nail manicure (Kanebo Cosmetics Inc., Japan), a resin

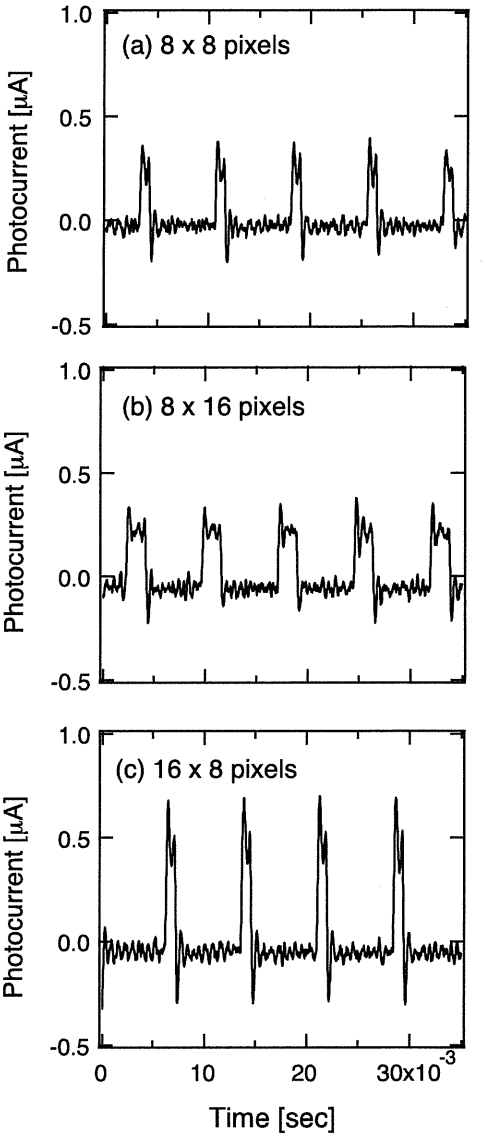

Fig. 2. Waveforms of photocurrent generated by various sizes of light spots on the display panel.

that changes the impedance on the sensing surface. To enhance the spatial resolution, scanning with a sub-pixel step was also tested. Each pixel on the OLED display consists of three sub-pixels of red (R), green (G), and blue (B), which are arranged horizontally in a sequence of *RGBRGB*... A light spot of 1 × 1 pixel can be moved at a step size of 1/3 pixel by turning on combinations of three sub-pixels in a sequence of (1) *RGBRGB*..., (2) *RGBRGB*..., (3) *RGBRGB*..., and (4) *RGBRGB*....

3. Results and discussion

3.1. Generation of photocurrent signal

To begin with, the waveform of the photocurrent signal induced by a light spot on the OLED display was examined. The upper panel of Fig. 2 shows a typical photocurrent induced by a light spot of 8 × 8 pixels in size. A waveform with a periodicity of about 7.4 ms was observed, which corresponded to the refresh rate of the display, 135 Hz. Within a light spot, pixels on the same line flash simultaneously and then pixels on the next line flash, and therefore, the

Please cite this article in press as: K. Miyamoto, et al., Miniaturized chemical imaging sensor system using an OLED display panel, Sens. Actuators B: Chem. (2012), doi:10.1016/j.snb.2011.02.029

waveform is a superposition of the pulsed photocurrent from all pixels turned on.

The waveforms of the photocurrent induced by different sizes of light spots were compared. The middle and bottom panels of Fig. 2 show the waveforms of photocurrent induced by a light spot of 8×16 and 16×8 pixels, respectively. In the case of 8×16 pixels, the light spot is longer in the vertical direction (the direction of refresh), and the duty cycle of the waveform becomes larger due to the time delay between lines. In the case of 16×8 pixels, the number of pixels simultaneously turned on is increased, and therefore, the amplitude of the photocurrent becomes larger while the duty cycle does not change.

3.2. pH response

In a LAPS measurement, the amplitude of the photocurrent is used as a sensor signal dependent on the width of the depletion layer, which responds to the potential of the sensor surface through the field effect. In Fig. 3(a), the amplitude of the photocurrent measured with a light spot of 9×9 pixels is plotted as a function of the bias voltage for various pH values. The amplitude of 135 Hz component in the photocurrent was calculated in the method described in our previous paper [12]. The shift of the current–voltage curve is observed, which is essentially the same as that of the conventional LAPS. In Fig. 3(b), this shift was plotted as a function of pH, and the sensitivity of the measurement was calculated to be 53.7 mV/pH, which was close to the Nernstian shift.

3.3. Chemical imaging

Fig. 4 shows an example of chemical images for different pH values. The resolution of the chemical image can be chosen by changing the size and the step of movement of the moving light spot. Images in Fig. 4 were obtained with a light spot of 4×4 pixels moved at a step size of 2 pixels. Thus, the resolution of the chemical image was 48×32 pixels. During the scan, the photocurrent was collected under a fixed bias voltage of −0.5 V, and the spatial distribution of the photocurrent value was represented as a chemical

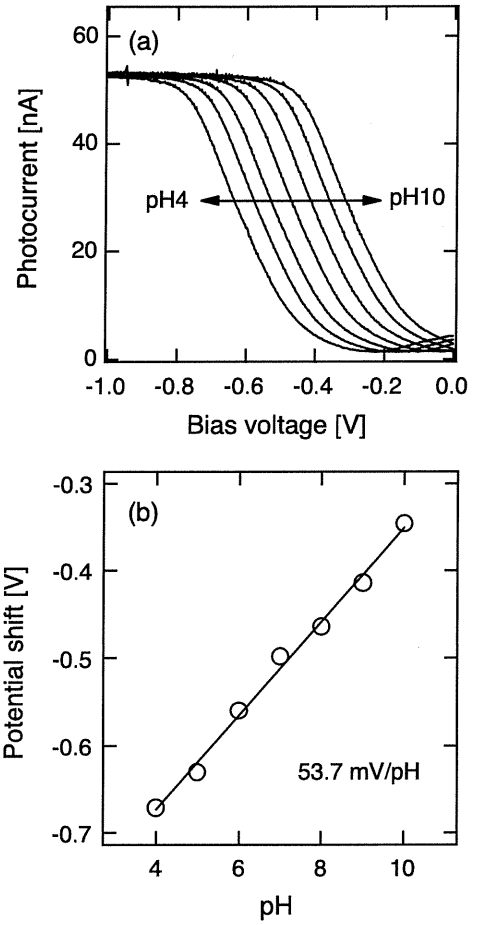

Fig. 3. (a) *I–V* curves and (b) the plot of their shift for various pH buffer solutions.

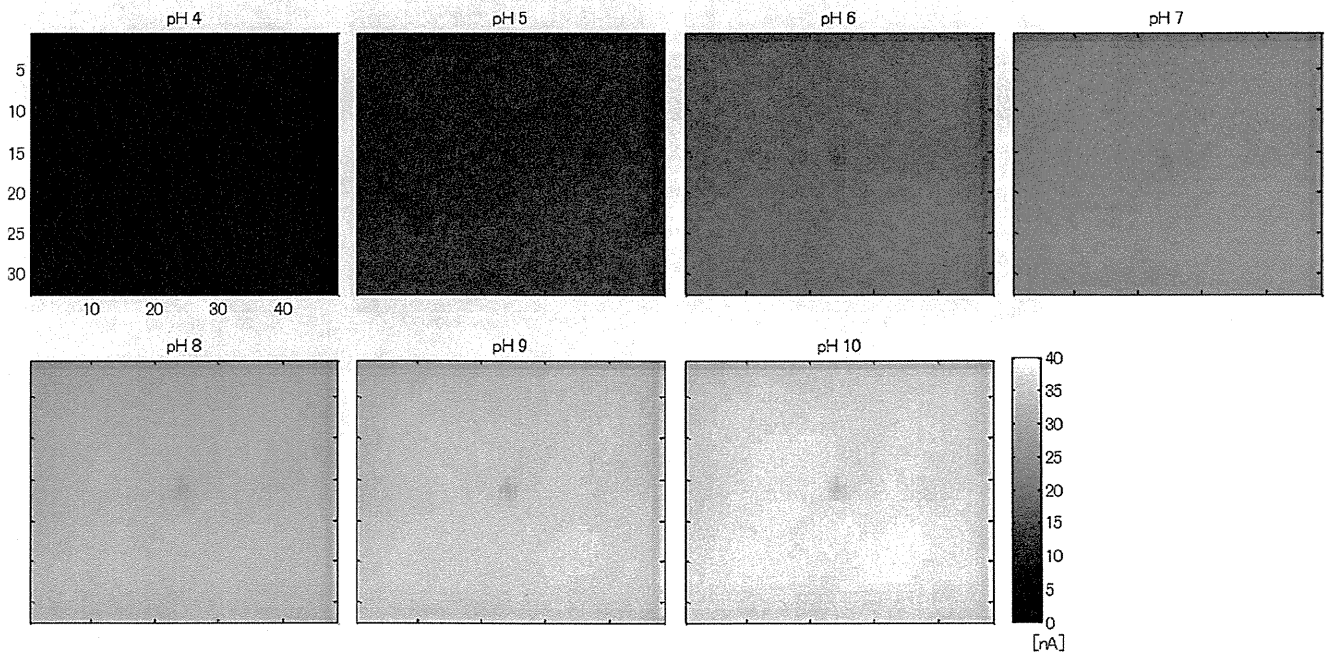

Fig. 4. Chemical images corresponding to different pH values. The sensing area was 20 mm × 14 mm, defined by the display size.

Please cite this article in press as: K. Miyamoto, et al., Miniaturized chemical imaging sensor system using an OLED display panel, Sens. Actuators B: Chem. (2012), doi:10.1016/j.snb.2011.02.029

image. The pH dependence of the photocurrent in Fig. 4 is consistent with Fig. 3(a), where the photocurrent decreases for lower pH values and increases for higher pH values under a fixed bias voltage.

Fig. 5 shows a variation of photocurrent–bias voltage characteristics obtained with different sizes of light spots with 8×8 to 1×1 pixels. The actual areas of the light spots were 1.6 mm × 1.6 mm to 200 μm × 200 μm. As can be seen in Fig. 5, the amplitude of the photocurrent increases with the size of the light spot. The photocurrent depends on the size of the illuminated area, and a better S/N ratio is expected for a higher photocurrent. As we used only square light spots, not only the amplitude but also the duty ratio of the photocurrent became larger for a larger size of light spot.

Fig. 6 compares the spatial resolution of chemical images of a test pattern scanned with different sizes of light spots. The size of the light spot was changed from 8×8 to 1×1 pixels and the step of movement was changed from 8 to 1 pixels, respectively. From the comparison of chemical images and the scales of the photocurrent in Fig. 6(b), the pixel-size dependence of the spatial resolution and the amplitude of the photocurrent is clearly observed. In the case of a light spot of 8×8 pixels moved at a step size of 8 pixels, the observed pattern was not clear, but the amplitude of the

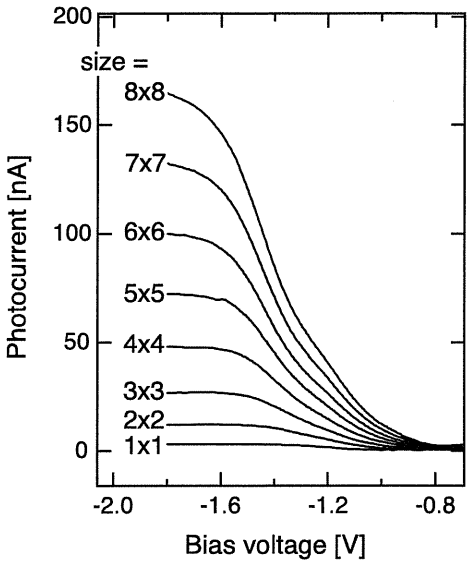

Fig. 5. Photocurrent characteristics obtained with different sizes of light spots.

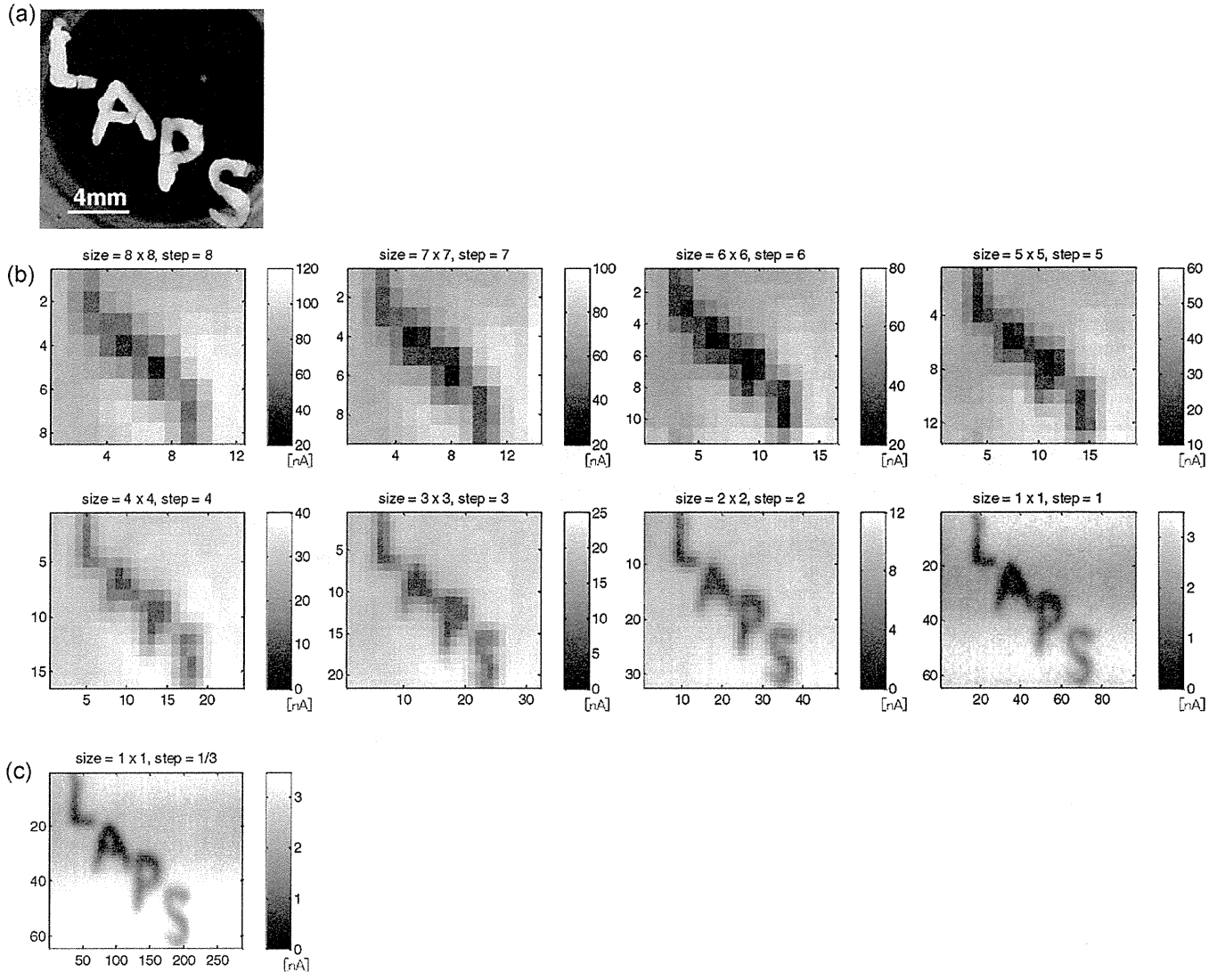

Fig. 6. (a) The alphabetic test pattern on the sensor surface. (b) Chemical images obtained with different sizes of light spots. (c) Chemical image with enhanced resolution obtained by scanning with a sub-pixel step size.

Please cite this article in press as: K. Miyamoto, et al., Miniaturized chemical imaging sensor system using an OLED display panel, Sens. Actuators B: Chem. (2012), doi:10.1016/j.snb.2011.02.029

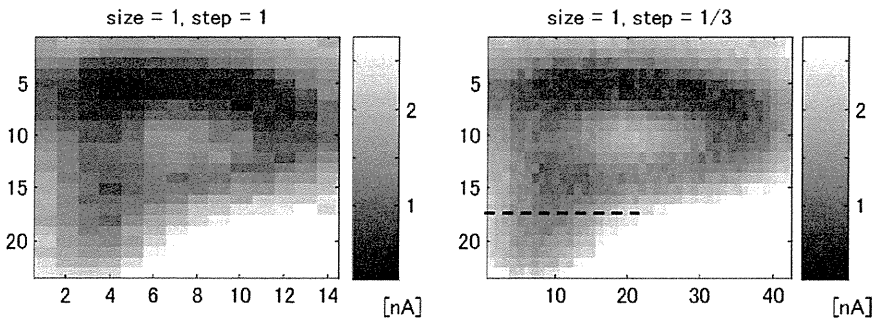

Fig. 7. Comparison of chemical images obtained by a light spot of 1 × 1 pixel moved at a step size of 1 pixel (left) and at a step size of 1/3 pixel (right).

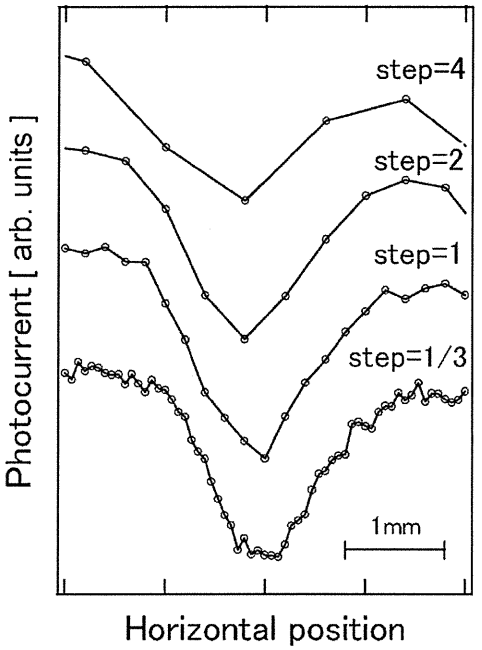

Fig. 8. Cross-sectional plot of photocurrent for various step sizes. The position corresponds to the dashed line on Fig. 7 right.

photocurrent was larger compared to others. On the other hand, in the case of a light spot of 1 × 1 pixel moved at a step size of 1 pixel, the alphabetic pattern is clearly resolved. In the chemical imaging based on OLED-LAPS, the spatial resolution depends both on the size of the light spot and the step size of movement.

In this experiment, we recorded the photocurrent for 1 s at each pixel. The long recording time of the photocurrent was due to the low refresh rate of the display. The total measurement time to obtain a single chemical image was 96 s, 384 s, and 1536 s for the spot sizes of 8, 4, and 2 pixels, respectively.

The resolution of chemical images in OLED-LAPS can be further enhanced by using sub-pixels. Fig. 6(c) shows a chemical image obtained by moving a light spot of 1 × 1 pixel at a step of 1/3 pixel in the horizontal direction. Fig. 7 compares the details of chemical images obtained with a light spot of 1 × 1 pixel moved at a step size of 1 pixel and at a step size of 1/3 pixel. Fig. 8 shows cross-sectional plots of the photocurrent values on the dashed line in Fig. 7 with various step sizes. It is clearly seen that the resolution in the horizontal direction is enhanced by using sub-pixels.

4. Conclusion

The novel OLED-LAPS measurement system was developed using a light spot on the OLED display as a light source. A periodic waveform of photocurrent was induced by the light from the OLED display with a refresh rate of 135 Hz. The amplitude and the duty cycle of the photocurrent changed depending on the horizontal and vertical dimension of the light spot on the display.

Measurement and visualization of pH by the OLED-LAPS system were demonstrated. The photocurrent–bias voltage characteristics shifted depending on the pH value of the sample. By moving the light spot on the display, chemical imaging was successfully achieved. The resolution and the S/N ratio of the chemical image were dependent on the pixel size of the light spot. An enhanced resolution was realized by using sub-pixels.

Since the new system based on OLED-LAPS does not require any complicated mechanism and optics, the measurement system is distinctly reduced in size in comparison to the conventional chemical imaging sensor systems [1,3]. In addition, the measured area defined by illumination can be arbitrarily customized to fit the size and shape of the sample to be investigated. A study on the application of the miniaturized OLED-LAPS system is in progress.

Acknowledgements

This work was supported by JSPS Grant-in-Aid for Scientific Research (B) (contract no. 19350036) and the Global COE Program "Global Nano-Biomedical Engineering Education and Research Network Centre", Tohoku University. K.M. acknowledges the support of JSPS Grant-in-Aid for Young Scientists (B) (contract no. 21750070). A part of this research was carried out at the Machine Shop Division of Fundamental Technology Center, Research Institute of Electrical Communication, Tohoku University.

References

[1] M. Nakao, T. Yoshinobu, H. Iwasaki, Scanning-laser-beam semiconductor pH-imaging sensor, Sens. Actuators B 20 (1994) 119–123.
[2] M. Nakao, S. Inoue, R. Oishi, T. Yoshinobu, H. Iwasaki, Observation of microorganism colonies using a scanning-laser-beam pH-sensing microscope, J. Ferment. Bioeng. 79 (1995) 163–166.
[3] S. Inoue, M. Nakao, T. Yoshinobu, H. Iwasaki, Chemical-imaging sensor using enzyme, Sens. Actuators B 32 (1996) 23–26.
[4] T. Yoshinobu, H. Iwasaki, Y. Ui, K. Furuichi, Y. Ermolenko, Y. Mourzina, T. Wagner, N. Näther, M.J. Schöning, The light-addressable potentiometric sensor for multi-ion sensing and imaging, Methods 37 (2005) 94–102.
[5] D.G. Hafeman, J.W. Parce, H.M. McConnell, Light-addressable potentiometric sensor for biochemical systems, Science 240 (1988) 1182–1185.
[6] T. Yoshinobu, T. Harada, H. Iwasaki, Application of the pH-imaging sensor to determining the diffusion coefficients of ions in electrolytic solutions, Jpn. J. Appl. Phys. 39 (2000) L318–L420.
[7] B. Stein, M. George, H.E. Gaub, J.C. Behrends, W.J. Parak, Spatially resolved monitoring of cellular metabolic activity with a semiconductor-based biosensor, Biosens. Bioelectron. 18 (2003) 31–41.
[8] Q. Liu, H. Cai, Y. Xu, L. Xiao, M. Yang, P. Wang, Detection of heavy metal toxicity using cardiac cell-based biosensor, Biosens. Bioelectron. 22 (2007) 3224–3229.
[9] D. Filippini, F. Winquist, I. Lundström, Computer screen photo-excited surface plasmon resonance imaging, Anal. Chim. Acta 625 (2008) 207–214.
[10] D. Filippini, S.P.S. Svensson, I. Lundström, Computer screen as a programmable light source for visible absorption characterization of (bio)chemical assays, Chem. Commun. (2003) 240–241.

Please cite this article in press as: K. Miyamoto, et al., Miniaturized chemical imaging sensor system using an OLED display panel, Sens. Actuators B: Chem. (2012), doi:10.1016/j.snb.2011.02.029

[11] K. Miyamoto, Y. Sugawara, S. Kanoh, T. Yoshinobu, T. Wagner, M.J. Schöning, Image correction method for the chemical imaging sensor, Sens. Actuators B 144 (2010) 344–348.
[12] K. Miyamoto, Y. Kuwabara, S. Kanoh, T. Yoshinobu, T. Wagner, M.J. Schöning, Chemical image scanner based on FDM-LAPS, Sens. Actuators B 137 (2009) 533–538.

Biographies

Ko-ichiro Miyamoto was born in Yamaguchi, Japan, in 1979. He received BE, ME, and PhD degrees from Tohoku University in 2002, 2004 and 2006, respectively. His PhD degree is for his study on the bio-molecular sensing using infrared absorption spectroscopy. Since 2006, he is an assistant professor in the Department of Electronic Engineering, Tohoku University. His research subject is on the application of silicon-based chemical sensors for bio-molecular sensing.

Kazumi Kaneko was born in Tochigi, Japan, in 1985. He received BE from Department of Electronic Engineering of Tohoku University in 2008, and also received ME from the Graduate School of Biomedical Engineering, Tohoku University in 2010. His research subject is also on the development of chemical image sensor based on the light-addressable potentiometric sensor.

Akira Matsuo was born in Ibaraki, Japan, in 1987. He received BE and ME from Department of Electronic Engineering of Tohoku University in 2010 and 2012, respectively. His research subject is on the development of chemical image sensor based on the light-addressable potentiometric sensor.

Torsten Wagner was born in Mönchengladbach, Germany, in 1978. He received his diploma in 2003 in electrical engineering from the University of Applied Sciences Aachen, his master of science in 2003 in model simulation and control from the Coventry University in UK, and his doctoral degree (PhD) in 2008 from the Philipps University Marburg in cooperation with the University of Applied Sciences Aachen. His research subjects concern chemical sensors, especially the light-addressable potentiometric sensor and sensor-signal processing. He received a scholarship (2008–2010) from the Japanese Society for the Promotion of Sciences (JSPS) to work at the Tohoku University in Japan, at which he became 2010 an assistant professor.

Shin'ichiro Kanoh was born in Kanagawa, Japan, in 1968. He received BE, ME, and PhD degrees in electric and telecommunication engineering from Tohoku University in 1991, 1993 and 1996, respectively. From 1996 to 2010, he was an assistant professor for electronic engineering at the Tohoku University, Sendai, Japan. He jointed Tohoku Institute of Technology in 2010. Since 2011, he is an associate professor in Tohoku Institute of Technology. His research subjects concern measurement and analysis of brain activities, biosignal measurement in general, and development of brain–computer interface.

Michael J. Schöning received his diploma degree in electrical engineering (1989) and his PhD in the field of semiconductor-based microsensors for the detection of ions in liquids (1993), both from the Karlsruhe University of Technology. In 1989, he jointed the Institute of Radiochemistry at the Research Centre Karlsruhe. Since 1993, he has been with the Institute of Thin Films and Interfaces (now, Institute of Bio and Nanosystems) at the Research Centre Jülich, and since 1999 he was appointed as full Professor at Aachen University of Applied Sciences, Campus Jülich. Since 2006, he serves as a director of the Peter-Grünberg Institute (PGI-8) at the Aachen University of Applied Sciences. His main research subjects concern silicon-based chemical and biological sensors, thin-film technologies, solid-state physics, microsystem and nano(bio-)technology.

Tatsuo Yoshinobu was born in Kyoto, Japan, in 1964. He received BE, ME, and PhD degrees in electrical engineering from Kyoto University in 1987, 1989, and 1992, respectively, for his study on gas source molecular beam epitaxy of siliconcarbide. In 1992, he joined the Institute of Scientific and Industrial Research, Osaka University, where he started the development of silicon-based chemical sensors. From 1999 to 2000, he was a guest scientist at the Research Centre Jülich, Germany. Since 2005, he is a professor for electronic engineering at Tohoku University, Sendai, Japan. Since 2008, he is also a professor at the Graduate School of Biomedical Engineering, Tohoku University.

Please cite this article in press as: K. Miyamoto, et al., Miniaturized chemical imaging sensor system using an OLED display panel, Sens. Actuators B: Chem. (2012), doi:10.1016/j.snb.2011.02.029

研究紹介

医療用中空光ファイバとその応用システム

松　浦　祐　司

細径内視鏡に光ファイバを挿入したレーザー内視鏡が，ヘルニアの除去や前立腺肥大の治療に実用化されているが，筆者らは，高エネルギー赤外光の伝送が可能な中空光ファイバを用いることにより，極めて高い効率で生体組織の蒸散などが可能な，波長2.94 μmのEr:YAGレーザーを用いた内視鏡レーザーシステムを実現した．また，人体に傷をつけない無侵襲な生体内組織診断である光バイオプシーのための技術として，悪性腫瘍の診断・早期発見や動脈硬化に伴う血管内壁の状態変化の診断などに有効な赤外分光法およびラマン分光法が挙げられるが，これらの両方に適用可能な光プローブとして，細径かつ柔軟な中空光ファイバを用いた分光システムを開発した．

Keywords : hollow optical fiber, infrared fiber, laser treatment, infrared spectroscopy, Raman spectroscopy

1.　赤外レーザー光伝送用中空光ファイバ

医療用途においては，赤外波長域のCO_2レーザー（波長10.6 μm）やEr:YAGレーザー（2.94 μm）が生体組織の水分に強く吸収される性質をもつため，高効率な生体組織蒸散が可能であり，レーザーメスや歯牙切削などに用いられる．一般的な光ファイバを構成する石英ガラスは，上記の中赤外光に対しては不透明であり，ファイバとして利用することはできないため，赤外光に対して極めて透明性の高い「空気」をコアとして光を伝送しようとするものが中空光ファイバである．中空光ファイバは細管状の導波路であり，通常の光ファイバとは対照的に，屈折率の低い空気をコアとし，高屈折率の誘電体や金属でクラッディングを構成したものである[1]．そのため，コアとクラッディングの境界面では全反射が生じず，光のエネルギーの一部は反射時に外部に漏れながらコア内を伝搬するが，伝送する光の波長においてファイバ内面での反射率を高めて，ほぼ100%に近づけることができれば，中空光ファイバにおいても低損失伝送が実現可能となる．その方法として，鏡面をもつ金属薄膜をガラスチューブの内面に形成し，さらにその表面に赤外域で透明な誘電体の薄膜を増反射コーティングとして形成する．

筆者らのグループにおけるファイバの製造工程は，金属層としての銀薄膜をチューブ内面に形成するための無電解メッキ法と，その表面に誘電体薄膜として，赤外波長域で透明性の高い環状オレフィンポリマー（COP）を形成するための送液法からなる[2]．

2.　レーザー内視鏡治療システムへの応用

細径内視鏡にガラス光ファイバを挿入し，波長1.06 μmのNd:YAGレーザーや2.1 μmのHo:YAGレーザーを患部に照射することにより，治療を行うことが可能なレーザー内視鏡が，ヘルニアの除去や前立腺肥大の治療に実用化されている．より長波長(2.94 μm)のEr:YAGレーザーが，その発振波長が水の吸収ピークに一致するために，極めて高い効率で生体組織の蒸散などが可能であることが報告されており[3]，筆者らはすでに歯科用レーザー治療装置として市場に普及しつつある中空光ファイバをEr:YAGレーザー光用の伝送路として利用し，内視鏡へ実装することを試みた．

図1は上記の手法でEr:YAGレーザー伝送用として設計・製作した，内径0.7 mm，長さ1 mのCOP中空ファイバの中赤外域における伝送損失スペクトルである．波長

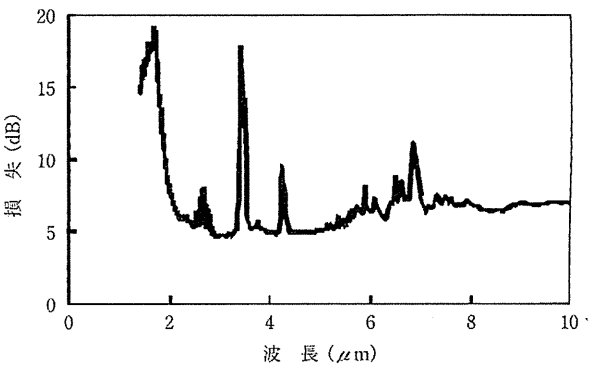

図1　中空光ファイバの損失スペクトル．

東北大学 大学院 医工学研究科　〒980-8579　仙台市青葉区荒巻字青葉6-6-05.　e-mail : yuji@ecei.tohoku.ac.jp　分類番号　6.7, 9.4
Hollow optical fibers for medical applications.　Yuji MATSUURA.　Graduate School of Biomedical Engineering, Tohoku University (6-6-05 Aoba, Aramaki, Sendai　980-8579)

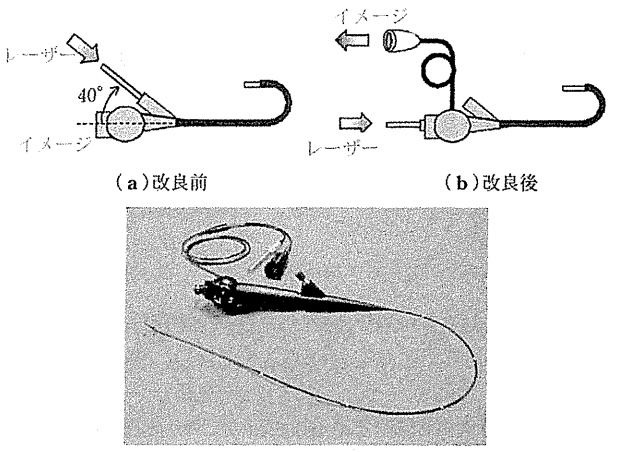

図2　中空光ファイバ用細径内視鏡の構造と外観.

3.5 μm と 7 μm 付近にポリマーの吸収による複数の損失ピークが見られるものの，目的とする波長 2.94 μm には目立った吸収は見られず，Er : YAG レーザーの伝送には影響が小さいことがわかる．一方，波長 1.5 μm の損失ピークはポリマー薄膜における光の干渉効果によるものであり，この効果により波長 3 μm 付近の損失が低減される．

泌尿器科用として使用されている先端部外径 2.7 mm の細径内視鏡を用い，この内視鏡の鉗子口（口径 1.2 mm）に，内径 0.7 mm，外径 0.9 mm の中空ファイバを挿入してレーザー伝送を行った．その場合，通常の内視鏡を用いると鉗子口にファイバを挿入する部分に比較的急峻な折れ曲がりが生じてしまい，このような曲げは付加損失の原因となってしまう．そこでこの影響を低減すべく，あらたに図2に示す構造の内視鏡を開発した．この内視鏡では柔軟なイメージファイバを曲げて側方に導き画像を観察し，中空ファイバは直線状態のまま，内視鏡の鉗子口へと挿入される．この改良の結果，内視鏡直線状態の場合でレーザー光透過率が 65% から 75% へ，先端を急峻に 180 度曲げた状態で 48% から 60% へと改善され，結石破砕に有効な 150 mJ 以上の出射エネルギーが得られた．開発した中空ファイバにより Er : YAG レーザー光を伝送し，人体から摘出した各種腎結石の破砕実験を行った結果を図3に示す．リン酸マグネシウムアンモニウム（MAP），リン酸カルシウム（CaP），炭酸カルシウム（$CaCO_3$）を主成分とする結石に 1 分程度のレーザー光を照射することにより，尿管から排出可能な，1.5 mm 以下の粒に破砕可能であることが示され，中空ファイバを用いた結石破砕術のもつポテンシャルが確認された．

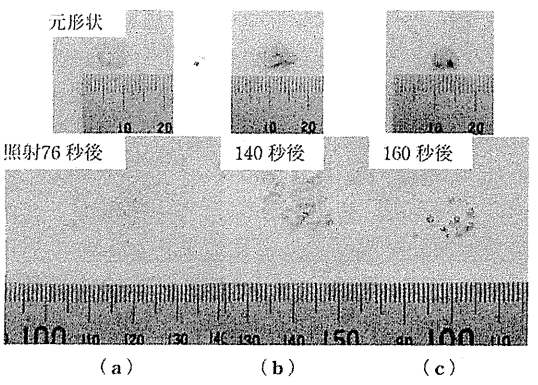

図3　各種結石に対するレーザー破砕の結果．主成分：(a) リン酸マグネシウムアンモニウム（MAP），(b) リン酸カルシウム（CaP），(c) 炭酸カルシウム（$CaCO_3$）.

3.　中空光ファイバを用いた分光バイオプシーシステム

3.1　赤外分光システム

近年の内視鏡技術と光応用技術の進歩に伴い，人体に傷をつけない無侵襲な生体内組織診断である光バイオプシーが注目されている．生体組織の分子構造や化学組成を分光法を用いて分析し，悪性腫瘍の診断・早期発見や動脈硬化に伴う血管内壁の状態変化の診断などに応用可能な技術として，赤外分光法とラマン分光法が挙げられる．赤外分光法に用いる光ファイバプローブとしてはこれまでに，カルコゲナイドガラスファイバ[4]や多結晶ファイバ[5]が赤外光用伝送路して開発されているが，材料の毒性や化学的耐久性に問題があり，医療への適用が難しかった．そこで本報告では，筆者らの研究グループで開発を行ってきた中空光ファイバをリモート赤外分光用プローブとして用いることを提案した[6]．

フーリエ変換赤外分光光度計（FTIR）を用いた分光反射スペクトル測定系を図4に示す．FTIR 内部のセラミック光源からの光は，金被膜軸外しミラーにより集光され，中空光ファイバ（内径 2 mm，長さ 1 m）に入射される．プローブとして使用した中空光ファイバは，生体組織の指紋領域となる波長 6〜15 μm において損失が低減されるように内装する COP の膜厚を 0.35 μm 前後に設定した．本ファイバは，柔軟なポリカーボネートチューブを母材としており，大口径化しても十分な可とう性を有し，その最小曲げ半径は 10 cm 程度である．また，曲率半径 20 cm 程度まで曲げた場合でも透過率の低下は全体の 5% 以内にとどまっており，この波長領域では曲げによる損失への影響が小さいこ

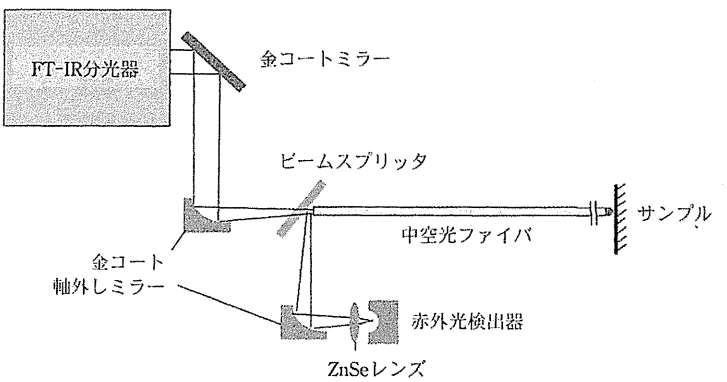

図4　赤外分光測定系.

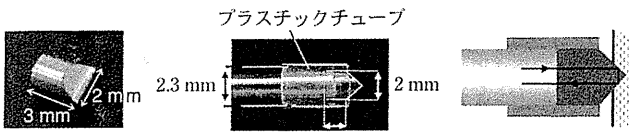

図5　シリコンATRプリズムの外観と光伝搬の様子.

とがわかった.

ファイバプローブの先端には図5に示すような構造のシリコン製減衰全反射（ATR）プリズムが取り付けられ，プリズム境界面で2回全反射する際に生じるエバネッセント波が，サンプル表面の吸収を検出する．中空光ファイバプローブは，前述のラマンプローブと同様に内視鏡やカテーテルに導入することにより，体内組織の分析をすることが可能である．図6は，中空光ファイバATRプローブを用いて測定した，ブタ腸壁摘出組織片サンプルの吸収スペクトルである．腸壁表面の異なる位置で取得されたスペクトルにおいて，コレステロールプラークの存在の有無により，脂質エステル（波長5.7 μm）の吸収の大きさには明らかな差異が表れている．この手法を用いて，血管内壁のコレステロール濃度分布を測定することが可能であり，人体から摘出したサンプルを用いて行った実験ではそのマッピングに成功している.

3.2　ラマン分光システム

ラマン分光法においては通常，励起光と検出光は可視もしくは近赤外光であるために，石英系のガラス光ファイバをプローブとして使用することができる．しかし，石英ガラスから発生するラマン散乱光の影響を除去するために，励起光用ファイバの出射端にはファイバからのラマン散乱光を取り除くためのバンドパスフィルタが，また散乱光検出用ファイバの入射端には，励起光を除去するための低域通過フィルタが必要となり，プローブ先端を細径化することは容易ではない[7].

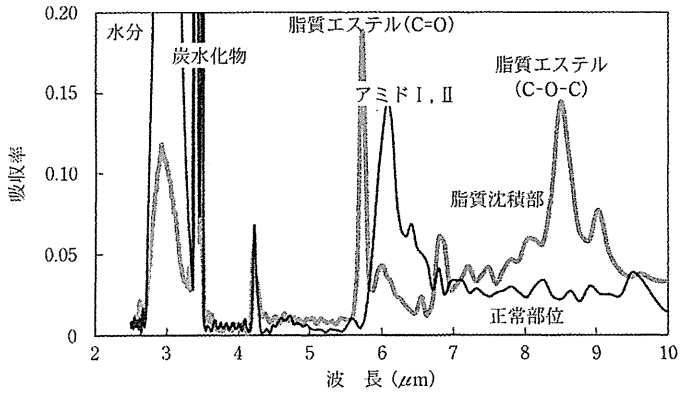

図6　ブタ腸壁の赤外吸収スペクトル.

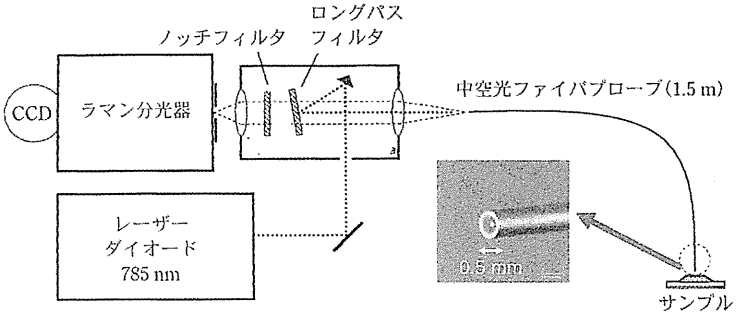

図7　ラマン分光測定系.

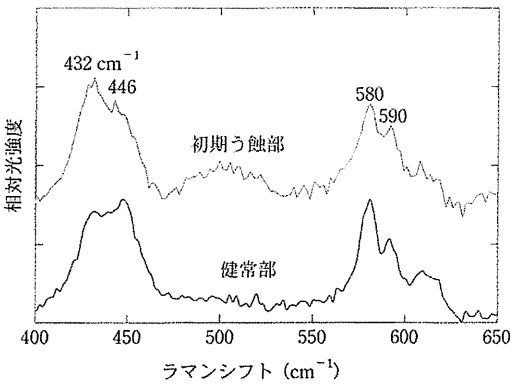

図8　初期う蝕部と健常部の歯牙表面のラマン散乱スペクトル.

そこで我々のグループでは，ラマン散乱を生じない空気をコアとする中空光ファイバをラマン分光用プローブとして用いることを提案した[8]．中空光ファイバはラマンノイズを発生しないため，その先端にフィルタを取り付ける必要がない．また，励起光と検出光の両方を単一のファイバで伝送することが可能なため，プローブの細径化が容易である．図7は中空光ファイバプローブを用いたラマン分光測定系の概要である．プローブとしては，ガラスキャピラリの内面に銀薄膜を形成した中空光ファイバ（内径320 μm，長さ1.5 m）を用い，その先端にはボールレンズが取り付けられている．励起光源としては波長785 nmのレーザーダイオードを用い，単レンズにより中空光ファイバへ結合している．中空光ファイバの実質的な開口角は全角で5°程度と極めて小さいため，焦点距離が150 mm程度のレンズを使用している.

中空光ファイバラマンプローブを用いて，抜去歯の健常なエナメル質部分および初期う蝕（虫歯）部分のラマンスペクトルを測定した結果を図8に示す[9]．432，446，580，590 cm^{-1}のピークはいずれも歯の主成分であるリン酸カルシウムのPO_4^{3-}のピークであるが，初期う蝕のスペクトルでは，エナメル質表面の結晶構造の変化により432 cm^{-1}および590 cm^{-1}のピークが増大していることが確認できる．ファイバを2次元的に走査しながらこのピーク強度比を測定することにより，初期う蝕部分をもつ抜去歯のラマンイメージング画像の取得を試みた．測定したラマンスペクトルの432 cm^{-1}/446 cm^{-1}のピーク強度比をプロットしたものを可視像

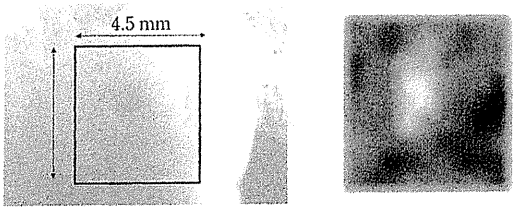

図9　う蝕のラマンイメージング結果.

とあわせて図9に示す．う蝕部分ではこのピーク強度比の値が大きくなるため，う蝕部分が検出できていることが確認できる．

4. むすび

当初，石英ガラス光ファイバが利用不可能な中赤外領域のレーザー光伝送用として開発された中空光ファイバは，ファイバの曲がりによる付加損失や，出射ビーム形状の変動など不可避な欠点も有するが，その高い耐久性や可とう性，人体への適合性などの大きな利点も有しており，内視鏡との組み合わせにより各種の分光用プローブとしての普及が期待される．応用分野は，本稿で述べた内視鏡下での赤外レーザー治療や赤外分光法を用いた低侵襲診断をはじめ，赤外光以外にも極端紫外や軟X線，またテラヘルツ領域へとさらに拡張する可能性を有している．また，石英ガラス光ファイバの損傷が問題となる高エネルギーナノ秒パルスや，同じく分散によるパルス延伸が生じるフェムト秒パルス伝送などにも対応が可能である．今後も引き続き，ファイバの更なる高効率化・細径化のために，ファイバの構造や製造法などについて検討を行っていく．

文　献

1) J. A. Harrington, ed.: *Infrared Fibers and Their Applications* (SPIE Press, 2003).
2) Y. Abe *et al.*: Opt. Lett. **23**, 89 (1998).
3) N. M. Fried *et al.*: Laser Surg. Med. **33**, 108 (2003).
4) A. B. Seddon: J. Non-Cryst. Solids **184**, 44 (1995).
5) D. A. Pinnow *et al.*: Appl. Phys. Lett. **33**, 28 (1978).
6) Y. Matsuura *et al.*: Appl. Opt. **48**, 5396 (2009).
7) Y. Komachi *et al.*: Opt. Lett. **30**, 2942 (2005).
8) 佐藤英俊ほか：光学 **35**, 521 (2006).
9) E. Yokoyama *et al.*: Appl. Opt. **47**, 4227 (2008).

(2011年8月2日　受理)

松浦　祐司（まつうら　ゆうじ）
1992年東北大学大学院工学研究科修了，博士（工学）．1993年住友電気工業研究員，94年米国ラトガース大学研究員として勤務の後，96年東北大学大学院工学研究科助教授．08年東北大学大学院医工学研究科教授．X線から遠赤外にわたる電磁波伝送路とその医療応用に関する研究に従事．

Microsyst Technol (2011) 17:1153–1160
DOI 10.1007/s00542-011-1267-1

TECHNICAL PAPER

Development of tactile sensor for measuring hair touch feeling

Takeshi Okuyama · Makoto Hariu · Tomoyuki Kawasoe · Minori Kakizawa · Hideki Shimizu · Mami Tanaka

Received: 5 September 2010 / Accepted: 3 March 2011 / Published online: 24 March 2011

Abstract In this paper, a tactile sensor system for evaluation of human hair under dry and wet conditions is developed. The polyvinylidene fluoride (PVDF) film is used as the sensory material. The sensor consists of an acrylic base, a silicone rubber, a PVDF film. A surface projection is put on the PVDF film as the contacting part. The sensor output is obtained by contacting and scanning objects. Panels imitating the physical and chemical properties of human hair surface are fabricated and used as measuring objects for stable measurement. Panels cleaned down with several kinds of hair-care products are measured by the sensor. By comparison between the sensor output and human sensory evaluation, it was confirmed that the sensor outputs have a good correlation with human sensory evaluation. It was found that the sensor system is available for monitoring hair conditions in both dry and wet conditions.

1 Introduction

Hair conditions are evaluated through the senses of sight and touch. For instance, touch feelings such as "roughness" and "smoothness" are perceived by the sense of touch. However, evaluations by the five human senses are highly dependent on subjectivity and experiences of people, so that it is difficult to express feelings quantitatively. Thus it has been expected to establish objective methods for evaluating touch feelings of human hair.

Currently research and development on devices and methods in order to evaluate physical properties of human hair have been conducted in various ways. With these devices and methods, it is possible to measure physical properties of human hair, such as surface friction (Bhushan et al. 2005), cross-section shapes (Wei et al. 2005), and bending stiffness (Baltenneck et al. 2001). However the results of the measurements do not necessarily correspond with the results of evaluation by human senses. Therefore, the evaluation of the touch feelings has been found to be difficult.

It is well-known that the human sense of touch recognizes about a few micrometers asperities owing to pacinian corpuscles, which is a sensory receptor in the dermis of skin (Shepherd 1994). Polyvinylidene fluoride (PVDF) film, which is a kind of piezoelectric material, has similar characteristics to those of pacinian corpuscles. Therefore, the film is useful for evaluating surface condition of soft objects (Tanaka and Numazawa 2004; Tanaka and Sugiura 2005; Dargahi et al. 2000). Tanaka et al. have developed a tactile sensor system for evaluations of human hair using the PVDF film as a sensory material (Tanaka et al. 2007). However, it was found that there is a problem that measurement values are not stable because human hair tends to be uneven and it is difficult to even out the overlaps of hair. Furthermore, evaluations of hair under wet conditions have not been conducted yet. Therefore, in order to reduce the individual variation in experiment, Kawasoe et al. have used the panels imitating the properties of hair surface, such as cuticle, in place of human hair for human sensory evaluation (Kawasoe et al. 2008). They have evaluated the influence of cuticle on the touch feelings of hair. It was found the hair damage feeling is obtained from the panel

T. Okuyama (✉) · M. Hariu · M. Tanaka
Tohoku University, 6-6-04, Aramaki-Aoba,
Aoba-ku, Sendai, Miyagi, Japan
e-mail: okuyama@rose.mech.tohoku.ac.jp

T. Kawasoe · M. Kakizawa · H. Shimizu
Shiseido Research Center, 2-12-1, Fukuura,
Kanazawa-ku, Yokohama, Kanagawa, Japan

with a wider cuticle and an irregular order of cuticle structure. It was confirmed that the panels are available at evaluating touch feeling of hair. However, objective evaluation with sensor system was not enough and touch feeling of panel treated hair-care products was not performed.

With these in mind, in this study, a PVDF sensor system for evaluating the touch feelings of hair is developed and touch feeling effect of hair-care products is evaluated by the sensor. The sensor consists of an acrylic plate, a silicone rubber sheet, and PVDF film. A projection is put on PVDF film. Firstly, panels that imitate aspects and properties of human hair surface are fabricated as measuring objects for stable measurement under dry and wet conditions. And two type sensors with different projection are fabricated. Next, the panels under dry and wet condition are evaluated by the developed sensors and human tactile sensation. And the performance of the sensors is investigated. Finally, the hair surface imitation panels treated with four pairs of hair-care products are evaluated by the sensor, and the capability of the sensor to evaluate the effect of hair-care products is investigated.

2 Hair surface imitation panels

Stable evaluation of human hair is difficult because of its unevenness and difficulty of putting it uniformly without overlaps. In addition, the touch feelings of hair remarkably change depending on the surrounding conditions such as temperature and humidity. Therefore, for stable evaluations, panels that imitate aspects and properties of the hair surface are used as measurement objects in this study.

Cuticles are the outermost layer of human hair surface (Robbins 2002). When people touch and feel hair, their hands directly contact the cuticles. However, the cuticles are easily striped off by brushing or by being exposed to ultraviolet rays. The damaged cuticles deteriorate hair gloss and touch feelings.

The surface shape of the cuticles, which affect the touch feelings of hair, is modeled as shown in Fig. 1 (Kawasoe et al. 2008). The widths and the heights of the surface shapes of the panels are listed in Table 1. Four kinds of panels are fabricated by Excimer laser. The panel is made of polyimide resin. Panel 1 imitates healthy hair, and Panel 2, 3, and 4 imitate damaged hairs. The surface shape of Panel 4 is designed by random combinations of the width

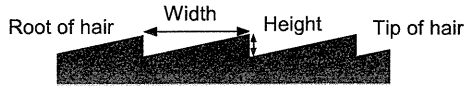

Fig. 1 Cross-section of surface pattern of hair surface imitation panel

Table 1 Properties of panels

Panel no.	1	2	3	4
Width (μm)	10	30	30	10–30
Height (μm)	1	1	5	1–3
Surface chemical activity	Hydrophobic	Hydrophilic		

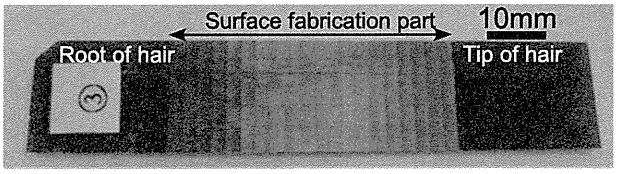

(a) Photograph of Panel 3

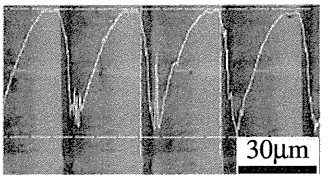

(b) Surface pattern on Panel 3 to imitate a damaged hair

Fig. 2 Panel 3 imitating surface of damaged hair

and the height within the ranges shown in Table 1. The difference in surface chemical activity of hair surface brings change of touch feeling according to the presence of water on hair. Therefore the panels imitate the surface chemical activity of hair too. Surface of Panel 1 is covered with hydrophobic layer to imitate healthy hair, and surfaces of the others are covered with hydrophilic layer. Figure 2 shows a photograph of Panel 3 and a close up picture of its processed part to imitate cuticles.

3 Sensor system for evaluation of touch feeling

3.1 Sensor structure and sensor system

Figure 3 shows the basic structure of the sensor. The sensor has a layered structure and consists of an acrylic plate, a silicone rubber sheet, and PVDF film whose surface is protectively coated with an acetate film. A projection is placed on the PVDF film. The projection contacts hair

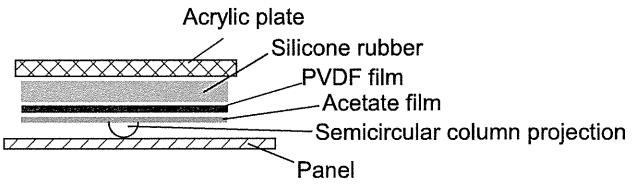

Fig. 3 Structure of the sensor

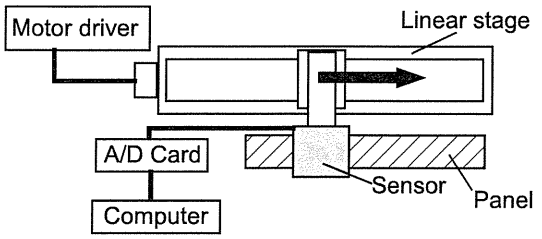

Fig. 4 Measurement system

surface imitation panels and transmits the panel surface conditions to the PVDF film. And then output voltages are obtained.

Figure 4 shows the developed measurement system. The PVDF sensor is mounted on the linear stage that is driven by a stepping motor, and the sensor is contacted to the processed part of the hair surface imitation panel. The sensor scans on the panel from hair root side to hair tip side, and outputs are obtained from the PVDF film. The obtained sensor outputs are put into a personal computer by an A/D card. Sampling frequency is 25 kHz, scanning begins 0.5 s after the beginning of a measurement, and the scanning speed is 50 mm/s. The scanning speed is decided with considering the human touch motion during feeling touch sensation.

3.2 Signal processing

According to previous studies (Tanaka and Numazawa 2004; Tanaka and Sugiura 2005), it was found that power spectrum density (PSD) of range from 100 to 500 Hz, which is corresponding to sensitive frequency range of pacinian corpuscles, and the variance of PVDF outputs are effective as a measuring parameter of human tactile sense. In this study, the unbiased variance of PVDF outputs (*VAR*) and the summation of PSD from 100 to 500 Hz (*FFT_AREA*) are used as evaluation parameters. The data of the section where the linear stage velocity changed is removed from the whole data, and evaluation parameters are calculated from only the data of the section where the device scans the processed part of panels at a constant speed.

The output *VAR* is calculated by the Eq. 1.

$$VAR = \frac{1}{N-1}\sum_{k=1}^{N}(Vo(k) - \overline{Vo})^2 \quad (1)$$

Here, N is the number of sensor output data using the calculation, $Vo(k)$ is kth PVDF output data, and $\overline{Vo}$ is the average of output $Vo(k)$.

The output *FFT_AREA* is obtained by the Eq. 2 with respect to calculated PSD by Fast Fourier Transform of PVDF outputs.

$$FFT\_AREA = \sum_{i=n1}^{n2} PSD(f_i)$$
$$(f_{n1} = 100 \text{ Hz and } f_{n2} = 500 \text{ Hz}) \quad (2)$$

Here, $PSD(f_i)$ is power spectrum density at the frequency of f_i Hz.

4 Evaluation of hair surface imitation panels

4.1 Sensory evaluation

Human sensory evaluations of Panels under dry condition, called "Dry", and wet condition, called "Wet", are carried out. "Wet" is a condition that three drops of water are put on the panel from a dropper.

Touch feeling is evaluated on a scale of 1–5. The evaluation value of Panel 3 is defined as the standard (value: "3"). If a panel has better touch feeling than Panel 3, the evaluation value is lower than "3", and if it feels worse, it is higher than "3". The subjects are 13 volunteers (four males and nine females). Four of them are evaluation experts.

The results of human sensory evaluations are shown in Table 2. From the results of "Dry", by comparison between Panel 2 and Panel 3, it was found that there is little difference in tactile feeling due to height differences. By comparison between Panel 1 and Panel 2, it was found that the touch feelings of panels get better with a decrease in the width of the imitation cuticle shape. Panel 4, which has a non-uniform height and width, is evaluated as the worst feeling. On the other hand, from the results of "Wet", Panel 1 is evaluated as the worst feeling although the panel is evaluated as the best feeling under "Dry". The change of touch feeling due to water is caused by the chemical activity of panel surface. It was confirmed that the panels can be used as alternative measuring objects for human hair.

4.2 Measurement by sensor

Hair surface imitation panels under "Dry" and "Wet" are measured by sensor. Two kinds of sensors with different projection are prepared (Table 3). As the semicircular column projection, Sensor 1 uses an acrylic column (radius: 1.5 mm) and Sensor 2 uses a vulcanized rubber

Table 2 Human sensory evaluation of panels

Panel no.	1	2	3	4
Dry	2.0	3.4	3.0	4.6
Wet	4.1	2.2	3.0	3.8

Table 3 Sensor projection type

	Sensor 1	Sensor 2
Material	Acrylic	Vulcanized rubber
Shape	Column	Column
Diameter	3 (mm)	3.5 (mm)

column (radius: 1.75 mm). Dimension of Sensor 2 is the same as that of Sensor 1, except for the projection part. The measurements are conducted five times for each condition. Figure 5 shows representative PVDF output waveforms and their PSD analysis for Panel 1 using sensor 2 under "Dry" and "Wet".

VAR and *FFT_AREA* are calculated from the PVDF outputs of measurement time from 0.6 to 1.3 s when the sensor scans stably on the processed part of hair surface imitation panel. Table 4 shows correlation coefficients between each parameter, *VAR* and *FFT_AREA*, and evaluation values by human sensory evaluation shown in Table 2. High correlations (0.9 or more) are indicated in boldface.

Focusing on Sensor 1, strong correlations of *FFT_AREA* were obtained under "Dry" and "Wet". However, Sensor 1 damaged the panel surface, because the projection of Sensor 1 is made of a relatively hard material. And it is not appropriate to repeated measurements.

Concerning with Sensor 2, strong correlations of *VAR* and *FFT_AREA* were obtained under "Dry". The sensor does not damage the panel. However, there are little correlations under "Wet". It is considered that the projection removes water drops from the panel like windshield wipers, because the projection is elastic cylindrical rubber. Furthermore, errors of sensor outputs on the same panel are small, and it is possible to easily distinguish each panel. From the results, experiments in the next section are carried out by Sensor 2.

5 Evaluation of effect of hair-care products

5.1 Treatment of hair surface imitation panel

Panel 4 is used for evaluating changes of the touch feeling of hair caused by hair-care products, because the panel is highly similar to damaged human hair. The panel is subjected to treatments shown in Table 5. In the experiments, four pairs of hair-care products (shampoos and conditioners A, B, C and D) are prepared. The panels subjected to Treatment S and SC are measured under wet conditions in order to estimate the sense of use. And dried panels (Treatment SCD) subjected to Treatment SC are evaluated, because the touch feeling of hair after drying is also important for hair-care products in order to estimate the sense of finish.

5.2 Sensory evaluation of hair surface imitation panels

The sensory evaluation is carried out on the panels treated with hair-care products by five female experts. Tables 6 and 7 show the results. Treatment S and Treatment SC are evaluated by five feelings: "Rough," "Slippery-smooth," "Smooth," "Squeak," and "Total feeling"(Table 6). Treatment SCD is evaluated by six feelings: "Rough," "Slippery-smooth," "Smooth," "Silky," "Moist," and "Total feeling." (Table 7) "Total feeling" asks whether the measuring object has a good touch feeling. Each feeling words is evaluated on a scale of 1–5. Higher evaluation value means that subjects obtain more of touch feeling expressed by the feeling word.

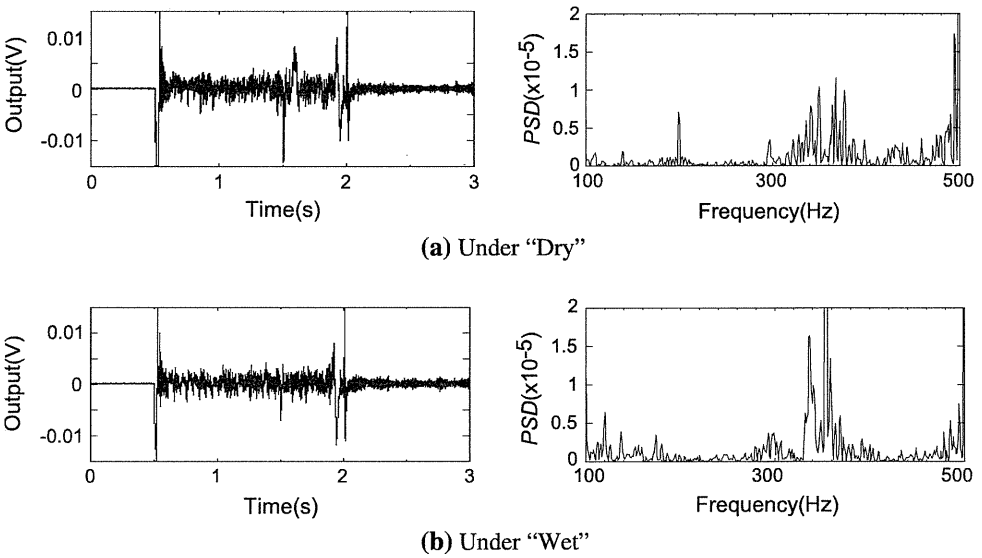

Fig. 5 Outputs of Sensor 2 for Panel 1

Table 4 Correlations between sensor outputs and human sensory evaluation

	Signal processing	Dry	Wet
Sensor 1	*VAR*	0.712	0.165
	FFT_AREA	**0.915**	**0.946**
Sensor 2	*VAR*	**0.983**	0.081
	FFT_AREA	**0.947**	0.194

Table 5 Methods of treatments

	Treatment
S	Three drops of water were dropped after the panel was washed with a shampoo
SC	Three drops of water were dropped after the panel was washed with a shampoo and conditioner
SCD	After "SC", the panel was dried

Table 6 Human sensory evaluations of panel with treatment "S" and "SC"

	Hair-care material	Rough	Slippery-smooth	Smooth	Squeak	Total feeling
S	A	3.1	2.7	2.7	3.6	2.3
	B	2.7	3.7	3.6	3.1	3.4
	C	2.5	4.0	3.8	2.5	3.9
	D	2.8	3.2	3.2	3.2	3.9
SC	A	3.3	2.5	2.4	3.7	2.5
	B	2.5	4.2	4.2	2.2	3.8
	C	2.6	3.8	3.7	2.7	3.8
	D	2.6	4.0	3.7	2.9	2.6

Table 7 Human sensory evaluations of panel with treatment SCD

Hair-care material	Rough	Slippery-smooth	Smooth	Silky	Moist	Total feeling
A	3.7	2.4	2.2	2.6	2.9	2.1
B	3.3	2.9	2.8	3.4	2.8	2.5
C	2.3	3.7	3.7	3.7	3.1	4.1
D	3.0	3.1	3.4	3.5	2.5	3.5

5.3 Measurement by sensor 2

Panels treated with hair-care products are measured using Sensor 2. Figure 6 shows representative output waveforms of panels with Treatment S, Treatment SC, and Treatment SCD using hair-care product A. Compared with sensor outputs of Treatment S, amplitudes of Treatment SC and Treatment SCD are small, so that it is inferred from the sensor outputs that changes in the surface conditions are affected by conditioner ingredients. By comparison

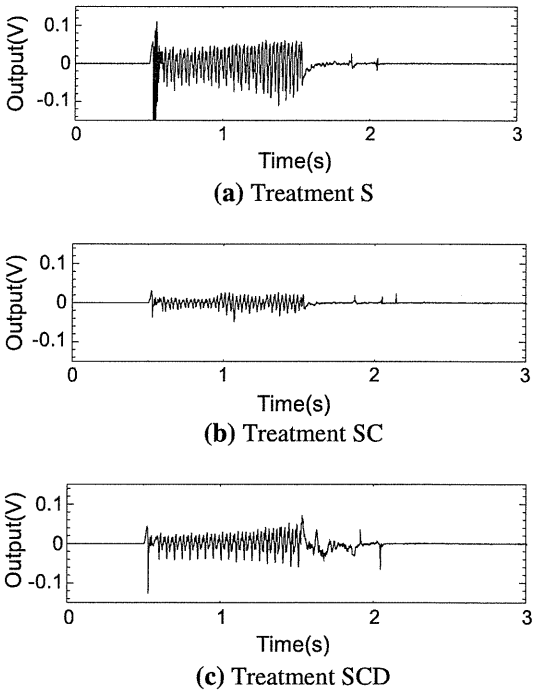

Fig. 6 Outputs of Sensor 2 for hair-care product A

between Treatment SC and Treatment SCD, differences in magnitude of amplitude were observed. Therefore, it is inferred that there are also changes in surface conditions under dry and wet conditions.

Next, *VAR* and *FFT_AREA* are obtained from PVDF output waveforms related to panels subjected to each treatment. And they are shown in Fig. 7. Differences of the effects due to each treatment can be seen more clearly in the figures, and these parameters are useful to distinguish differences in the sense of use and finish. The sensor can distinguish differences in touch feelings due to each shampoo and conditioner. It is considered that evaluation of hair-care products is possible to use the sensor system, because differences in parameter values are recognized.

5.4 Comparison between sensory evaluation and sensor measurement

Tables 8 and 9 summarize correlation coefficients between each parameter (*VAR* and *FFT_AREA*) calculated from sensor outputs and the results of human sensory evaluation shown in Tables 6 and 7. Table 8 shows correlation coefficients of panels subjected to Treatment S and Treatment SC. Table 9 shows correlation coefficients of panels subjected to Treatment SCD. High correlations (more than 0.7 or less than −0.7) are indicated in boldface.

VAR has no correlation with feelings of Treatment S and SC. However, *FFT_AREA* has a correlation only with "Rough" of Treatment S. At the same time, *VAR* and

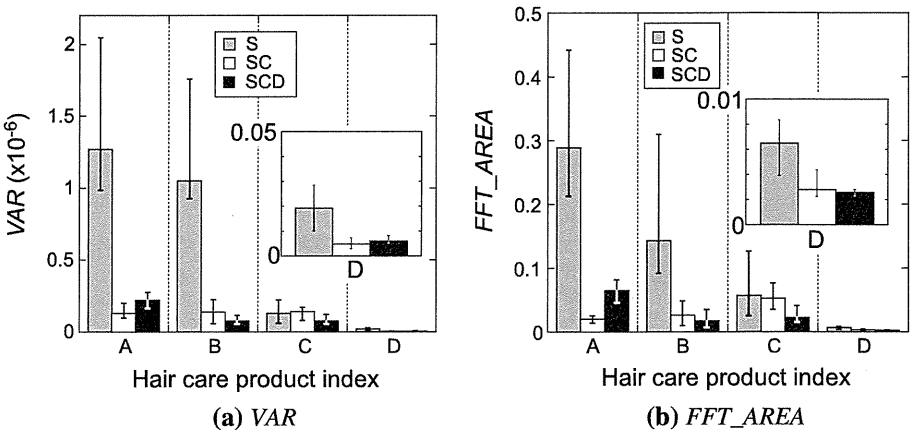

Fig. 7 The calculated parameter for treatment with each hair-care products using Sensor 2

Table 8 Correlations between human sensory evaluation and sensor output of Sensor 2 using panel with "S" and "SC"

	Signal processing	Rough	Slippery-smooth	Smooth	Squeak	Total feeling
S	*VAR*	0.627	−0.459	−0.481	0.646	−0.512
	FFT_AREA	**0.730**	−0.597	−0.639	0.659	−0.623
SC	*VAR*	0.586	−0.543	−0.430	0.265	−0.124
	FFT_AREA	−0.165	0.0558	0.151	−0.262	0.743

Table 9 Correlations between human sensory evaluation and sensor output of Sensor 2 using panel with "SCD"

Signal processing	Rough	Slippery-smooth	Smooth	Silky	Moist	Total feeling
VAR	0.625	−0.660	**−0.810**	**−0.883**	0.493	−0.652
FFT_AREA	0.594	−0.639	**−0.777**	**−0.885**	0.482	−0.604

FFT_AREA are highly correlated with "Silky" and "Smooth" of the panel was subjected to Treatment SCD.

The results show that hair surface imitation panels and the measuring system using a PVDF sensor are useful for evaluating hair-care products under "Dry" conditions. However, it was found that evaluation under "Wet" is difficult. As mentioned in the previous section, it is inferred that measurements under "Wet" are difficult because the projection removes water drops from the panel like windshield wipers during the measurements. Therefore, the projection and structure of the sensor are improved for measurement under "Wet" in the next section.

6 Evaluation by an advanced sensor

6.1 Sensor improvement

For successful evaluation of panels under "Wet", the surface projection shape of the sensor and the sensor structure are improved. The same experiment as the previous section is conducted by using the improved sensor and the validity of the sensor is investigated.

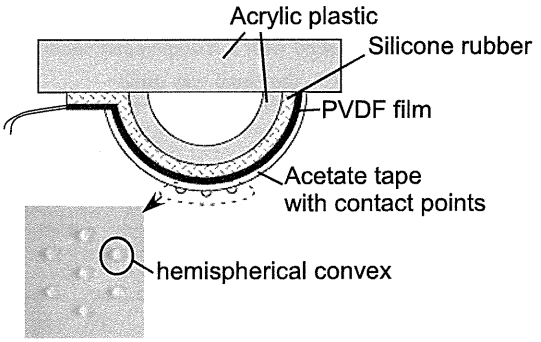

Fig. 8 Structure of sensor 3

Figure 8 shows the structure of the improved sensor. A new shape of the projection is required not to wipe out water drops on the panels. Therefore, a surface projection that seven hemispherical convex are placed on an acetate film is developed. The sensor is called Sensor 3. The hemispherical convex are placed on each vertex and the center of a regular hexagon with a side length of 3 cm. Due to space between each convex, measurements can be performed under "Wet" without wiping out drops of water.

The sensor surface projection, made of UV curable resin, is fabricated directly on the acetate film. Material of the projection is urethane acrylate resin. They are 0.25 mm in height and 1.0 mm in diameter. Because the height of the improved surface projection is less than one-tenth of that of Sensor 2, the sensor structure is improved so that the measurement can be made under the condition that only surface projection contacts panels. A silicon rubber and a PVDF film are set on an acrylic half-cylinder and a projection is mounted on the surface.

6.2 Measurement of effects of hair-care products

The same experiment as that using Sensor 2 is carried out by using Sensor 3. The results of measurements using

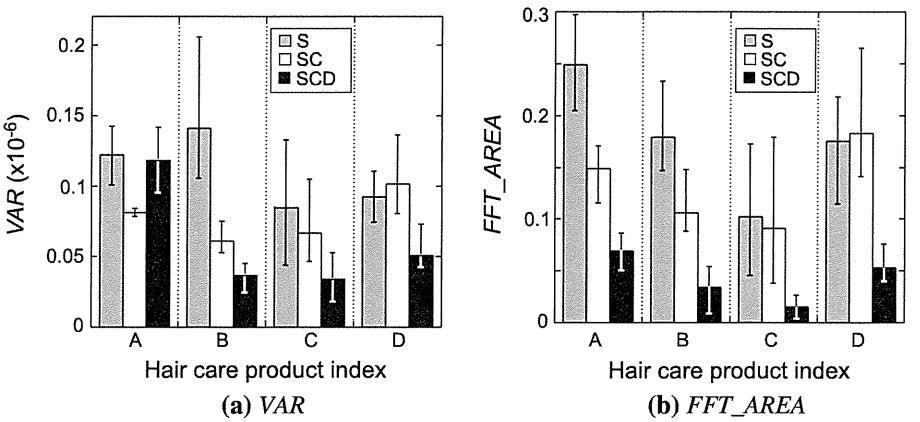

Fig. 9 The calculated parameter for treatment with each hair-care products using Sensor 3

(a) *VAR* (b) *FFT_AREA*

Table 10 Correlations between human sensory evaluation and sensor output of Sensor 3 using panel with "S" and "SC"

	Signal processing	Rough	Slippery-smooth	Smooth	Squeak	Total feeling
S	*VAR*	0.416	−0.243	−0.235	0.546	−0.320
	FFT_AREA	**0.974**	**−0.918**	**−0.914**	**0.987**	**−0.946**
SC	*VAR*	0.218	−0.165	−0.318	0.499	**−0.839**
	FFT_AREA	0.305	−0.225	−0.357	0.507	**−0.895**

Table 11 Correlations between human sensory evaluation and sensor output of Sensor 3 using panel with "SCD"

Signal processing	Rough	Slippery-smooth	Smooth	Silky	Moist	Total feeling
VAR	**0.745**	**−0.811**	**−0.809**	**−0.965**	0.028	−0.660
FFT_AREA	**0.839**	**−0.888**	**−0.749**	**−0.840**	−0.495	**−0.704**

Sensor 3 are compared with the results of sensory evaluation obtained in the previous chapter and correlations between them are calculated.

Figure 9 shows the results of *VAR* and *FFT_AREA*. From the results, it was found that changing tendencies of *VAR* and *FFT_AREA* for each product are different from those using sensor 2.

Tables 10 and 11 show correlations between the results of human sensory evaluation shown in Tables 6 and 7 and the results of measurement by Sensor 3 shown in Fig. 9. Table 10 is the results for Treatment S and Treatment SC and Table 11 is the results for Treatment SCD. High correlations (more than 0.7 or less than −0.7) are indicated in boldface.

Table 10 shows *FFT_AREA* of Treatment S is highly correlated to all feelings. In terms of Treatment SC, it was confirmed that both of *VAR* and *FFT_AREA* have strong correlations with "Total feeling". These results show that due to the improvement of the shape of a sensor surface projection, panel surfaces under wet conditions can be evaluated better than Sensor 2. At the same time, Table 11 shows evaluation by Sensor 3 has higher correlations with most feelings than that by Sensor 2 and it also shows the shape of Sensor 3 is more useful under dry conditions.

In consequence, it was found that the measurement results by using Sensor 3 and the results of human sensory evaluation have strong correlations with some of feelings regardless of conditions of panel surfaces. The developed sensor system is available for measurement of touch feelings of hair and for evaluation of the effects of hair-care products.

7 Conclusions

In this study, we developed a sensor system for evaluating the touch feelings of hair that is capable to make a stable evaluation under dry and wet conditions. And the results of the measurement of hair surface imitation panels treated with hair-care products showed strong correlations with sensory evaluation under dry and wet conditions. It was found that the sensor can evaluate the difference of touch feeling due to hair-care products. The developed sensor system was proved to be useful for measuring the touch feelings under dry and wet conditions.

References

Baltenneck F, Franbourg A, Leroy F, Mandon M, Vayssie C (2001) A new approach to the bending properties of hair fibers. J Cosmet Sci 52:355–368

Bhushan B, Wei G, Haddad P (2005) Friction and wear studies of human hair and skin. Wear 259:1012–1021

Dargahi J, Parameswaran M, Payandeh S (2000) A micromachined piezoelectric tactile sensor for an endoscopic grasper—theory, fabrication and experiments. J Microelectromech Syst 9(3):329–335

Kawasoe T, Kakizawa M, Shimizu H (2008) Tribology in the hair surface and tactile perception. Tribology Online 3(2):127–130

Robbins CR (2002) Chemical and Physical Behavior of Human Hair, 4th edn. Springer, New York, pp 386–469

Shepherd GM (1994) Neurobiology, 3rd edn. Oxford University Press, New York, pp 272–273

Tanaka M, Numazawa Y (2004) Rating and valuation of human haptic sensation. Int J Appl Electromagnetics and Mechanics 19:573–579

Tanaka M, Sugiura H (2005) Active haptic sensation for monitoring skin conditions. J Mater Process Technol 161:199–203

Tanaka M, Shimizu H, Kawasoe T (2007) International patent disclosure. WO2007/108318 A1

Wei G, Bhushan B, Torgerson PM (2005) Nanomechanical characterization of human hair using nanoindentation and SEM. Ultramicroscopy 105:248–266

J Mater Sci (2012) 47:1852–1859
DOI 10.1007/s10853-011-5972-z

Fabrication and fluorescence properties of multilayered core–shell particles composed of quantum dot, gadolinium compound, and silica

Yoshio Kobayashi · Takuya Nozawa · Tomohiko Nakagawa · Kohsuke Gonda · Motohiro Takeda · Noriaki Ohuchi

Received: 27 June 2011 / Accepted: 16 September 2011 / Published online: 1 October 2011

Abstract A preparation method for multilayered quantum dot/silica/gadolinium compound/silica (QD/Si/Gd/Si) core–shell particles is proposed. Silica (Si)-coated quantum dot (QD/Si) core–shell particles were prepared by a Stöber method at room temperature in water/ethanol solution with TEOS and NaOH in the presence of QD nanoparticles. Succeeding gadolinium compound (Gd)-coating of the QD/Si core–shell particles was performed by a homogeneous precipitation method using $Gd(NO_3)_3$, urea, and polyvinylpyrrolidone in the presence of the QD/Si particles, which resulted in production of multilayered QD/silica/gadolinium compound (QD/Si/Gd) core–shell particles. For Si-coating of the QD/Si/Gd particles, the Stöber method was performed at room temperature in water/ethanol solution with TEOS and NaOH in the presence of the QD/Si/Gd particles. Consequently, Si-coated QD/Si/Gd, i.e., multilayered QD/Si/Gd/Si, core–shell particles were obtained. The QD/Si/Gd/Si particles revealed strong fluorescence, which was almost comparable to the QD particles with no shells. These particles are expected to be harmless to living bodies, and have dual functions of magnetic resonance imaging and fluorescence.

Introduction

Imaging by using magnetic resonance (MR) is focused as an advanced technique for medical diagnosis [1–3]. Tissues in living bodies can be imaged with high contrast using gadolinium compounds (Gd) in MR imaging (MRI) because of their paramagnetism. Some gadolinium complexes are commercially available as MRI contrast agents. The MRI contrast agents are liquid solutions dissolving the gadolinium complexes. The gadolinium complexes face at a problem for difficulty in obtaining clear images for a long period because of their short residence time in living bodies. Formation of Gd nanoparticles can solve the problem. Nanoparticles have a projected area larger than molecules, so that flow of nanoparticles will be more controlled, i.e., their residence time will be prolonged.

The gadolinium complexes have another problem. They may release free gadolinium ions through dissociation of the complexes, and then the gadolinium ions may provoke adverse reactions in some patients [4, 5], so that the gadolinium complexes cannot be administered to such people. Among various methods for reducing adverse reactions derived from gadolinium complexes, coating of Gd nanoparticles (core) with materials inert to living bodies (shell) is a good candidate, because the shell materials prevent the Gd from contacting living bodies. Studies on coating of nanoparticles with silica (Si), which is inert to living bodies, have been extensively conducted [6–14]. They are techniques based on a sol–gel reaction of silicon alkoxide. We have also proposed methods for Si-coating of various materials [15–31].

Y. Kobayashi (✉) · T. Nozawa
Department of Biomolecular Functional Engineering, College of Engineering, Ibaraki University, 4-12-1 Naka-narusawa-cho, Hitachi, Ibaraki 316-8511, Japan
e-mail: ykoba@mx.ibaraki.ac.jp

T. Nakagawa · K. Gonda · M. Takeda · N. Ohuchi
Department of Nano-Medical Science, Graduate School of Medicine, Tohoku University, Seiryo-machi, Aoba-ku, Sendai 980-8575, Japan

N. Ohuchi
Department of Surgical Oncology, Graduate School of Medicine, Tohoku University, Seiryo-machi, Aoba-ku, Sendai 980-8574, Japan

Fluorescence imaging has been also performed in the field of medical diagnosis [32–34]. Cadmium compound (Cd) semiconductors have been widely used as a fluorescent marker, i.e., an imaging agent for the medical examination, because of their size-tunable photoluminescence, high brightness, and exceptional photostability [34, 35]. Colloid solutions of Cd nanoparticles are commercially available as the fluorescent marker by the name of "quantum dots (QD)." It is well known that Cd is harmful to living bodies. Its harm may also be reduced with the Si-coating.

Materials composed of components that have different properties should have multiple functions. Composite particles with magnetism and fluorescence have been of great interest in applications such as cell labeling [36–39], biosensing [40], and diagnostic medical devices [41, 42]. Based on the viewpoint for multi-functionalization of materials, particles containing QD and Gd will act as both the fluorescent marker and the MRI contrast agent.

This study proposes a method for preparing multilayered core–shell particles composed of core of QD, the first shell of silica, the second shell of Gd, and the third shell of Si. QD nanoparticles were Si-coated with a modified Stöber method (QD/Si particles), the QD/Si particles were coated with Gd using a homogeneous precipitation method (QD/Si/Gd particles), and then the QD/Si/Gd particles were Si-coated with a modified Stöber method (QD/Si/Gd/Si particles). In this study, their fluorescence property was also studied toward materials with dual functions.

Materials and methods

Materials

Quantum dot nanoparticles used were Qdot® (Invitrogen Co.) with a catalog number of Q21371MP. The QD nanoparticles are $CdSe_xTe_{1-x}$ nanoparticles coated with ZnS and successively surface-modified with carboxyl groups, and their concentration is 8×10^{-6} M. Figure 1a shows a transmission electron microscope (TEM) image of the QD nanoparticles. The QD nanoparticles had an average size of 10.3 ± 2.2 nm. Tetraethylorthosilicate (TEOS) (95%), sodium hydroxide (NaOH) solution (5 M), and ethanol (99.5%) were used as a Si source, a catalyst and a solvent in Si-coating by a sol–gel reaction of TEOS, respectively. Gadolinium nitrate hexahydrate ($Gd(NO_3)_3 \cdot 6H_2O$) (99.5%) and urea (99.0%) were used as chemicals for Gd compound shell and a precipitation-inducer for Gd-coating, respectively. Stabilizers used in the Gd-coating were *n*-hexadecyltrimethylammoniumbromide (CTAB) (96%), polyvinylpyrrolidinone (PVP) (M_w: 40,000), and sodium *n*-dodecyl sulfate (SDS). Except for the QD nanoparticles, all the other chemicals were purchased from Kanto Chemical Co., Inc., and were used as received. Water that was ion-exchanged and distilled with Shimadzu SWAC-500 was used in all the preparations.

Synthesis of particles

QD/Si particles

According to our previous study [28], QD/Si particles were prepared in a 10-mL glass vessel under vigorous stirring with a modified Stöber method. The Stöber method is based on hydrolysis and condensation of TEOS in the presence of ammonia as a catalyst in ethanol [43–45]. Since, amines such as ammonia are harmful to the human body [46, 47], NaOH was used as a catalyst for the hydrolysis and condensation of TEOS instead of ammonia in the modified Stöber method. To the colloid of QD nanoparticles were added water/ethanol solution and successively TEOS/ethanol solution. Then, the Si-coating was initiated by rapidly injecting 0.1 M NaOH aqueous solution into the QD/TEOS colloid solution. The Si-coating was performed for 24 h at room temperature. A total volume of the solution was 5 mL, and initial concentrations of QDs, H_2O, NaOH, and TEOS were 6.4×10^{-9}, 5, 4×10^{-4}, and 5×10^{-4} M, respectively. Figure 1b shows a TEM image of the QD/Si particles. The QD/Si particles had an average size of 20.1 ± 2.4 nm.

QD/Si/Gd particles

Gd-coating of the QD/Si particles was performed by a NaOH-addition method and a homogeneous precipitation method in the presence of the QD/Si particles, in a 10-mL glass vessel under active stirring.

In the NaOH-addition method, the Gd-coating was performed in 1:1 (v/v) water/ethanol solution. To water were added the as-prepared QD/Si particle colloid solution and ethanol. After 15 min, to the mixture successively added were the $Gd(NO_3)_3$ aqueous solution and 0.1 M NaOH aqueous solution (for adjusting initial pH to ca. 10.5). The reaction was carried out at room temperature for 24 h. A total volume of the solution was 5 mL, and initial concentrations of QD and $Gd(NO_3)_3$ were 3.2×10^{-9} and 3×10^{-4} M, respectively.

In the homogeneous precipitation, the Gd-coating was performed in 1:1 (v/v) water/ethanol solution at initial concentrations of 3.2×10^{-9} M QD, 1 g/L stabilizer, 0.5 M urea, and 3×10^{-5}–3×10^{-3} M $Gd(NO_3)_3$. To water successively added were the as-prepared QD/Si particle colloid solution, ethanol, and stabilizer aqueous solution. After 15 min, to the mixture successively added were urea aqueous solution, nitric acid (for adjusting pH to 5), and aqueous $Gd(NO_3)_3$. The mixture was stirred at 300 rpm and 60 °C for 6 h.